J. Fluid Mech. (1975), *vol.* 71, *part* 2, *pp.* 293–304
Printed in Great Britain

A study of the freezing of sea water

By R. FARHADIEH AND R. S. TANKIN
Gas Dynamics Laboratory, Northwestern University, Evanston, Illinois 60201

(Received 19 August 1974)

A Mach–Zehnder interferometer was used to study the interaction between convection currents in the sea water and the ice–water interface during freezing. The temperature at the ice–water interface during the early stages of freezing was approximately 0 °C, not the equilibrium freezing temperature. Salt plumes were observed to appear first at specific sites on the ice–water interface. This is contrary to earlier results reported by Farhadieh & Tankin (1972). The salinity profiles in the salt plumes were measured using interferograms in conjunction with Abel inversion. The maximum salinity, along the centre-line of the salt plume, is an indication of the salinity of the brine trapped within the ice.

1. Introduction

The purpose of this study is to investigate the freezing of sea water under various conditions. This study is an extension of earlier work (Tankin & Farhadieh 1971; Farhadieh & Tankin 1972, 1974). Particular attention is focused on the interaction between the thermal convective currents in the sea water and the ice–water interface during the early stages of freezing and on the salt plumes that appear in the sea water during the later stages of freezing.

Freezing in the presence of convective currents has not been widely studied, however a few pertinent papers will be mentioned. Townsend (1964), using a thermistor probe, measured temperature profiles in fresh water where freezing was from below. He observed an unstable layer in the water above the ice–water interface which extended to about the 3·2 °C isotherm; above this region, there were fluctuations in temperature attributed to internal gravity waves. Tien & Yen (1966) and Yen (1968) focused their attention on various heat-transfer properties, such as temperature profiles in the water, ahead of the ice–water interface, the Nusselt number and the critical Rayleigh number. Boger & Westwater (1967) studied the effect of buoyancy forces on melting and freezing, and Heitz & Westwater (1971) studied melting in containers having various aspect ratios. All of these measurements are concerned with the steady advance of the ice front, not the initial formation of the ice front and its development shortly after freezing began. Foster (1969) observed salt plumes during the freezing of sea water using a schlieren optical system. In his experiment, thermal convection currents were not present in the sea water below the ice–water interface because he maintained the sea water at a Rayleigh number below the critical value.

In the present study, coupling between the thermal convective currents and the ice–water interface was observed. This has also been reported in earlier papers

by Tankin & Farhadieh (1971) and Farhadieh & Tankin (1972). In the latter paper, involving sea water, the experiments were highly transient, which may have led to errors in the interpretation of the data. However, the conclusions of that paper are consistent with those of the present study. In the earlier experiments, a large heat flux was suddenly imposed at the top plate to establish a convection pattern and eventual freezing. The interferograms show a series of fringes having closed contours. For two-dimensional rolls, which were assumed, the fringes represent isotherms. Thus closed contours would mean localized regions of hot and cold fluid within the test section, which is impossible under steady-state conditions. The time-dependent numerical solution for the development of Bénard cells by Royal (1969), which corresponds to the transient experiment, does not yield closed isotherms. In the present series of experiments, great care was taken to establish the convective pattern (rolls) before freezing was induced. The heat flux through the top and bottom plates (opposite) was increased in small increments until the convection became relatively intense. The temperature of the top plate was near the freezing temperature when a large heat flux was applied to it to induce freezing. No closed fringes were observed in these experiments, and, on the basis of a recent paper by Farhadieh & Tankin (1974), two-dimensional rolls were indeed present in the test section. The first salt plumes to appear in the test section always occurred at a specific site (peak) on the ice–water interface. This is contrary to the observation reported by Farhadieh & Tankin (1972), which is further evidence that rolls were not present in that study. A special technique was used to obtain the salinity profiles within the salt plumes, which had not been measured previously.

2. Apparatus and experimental procedure

The optical set-up and the test section have been adequately described by Tankin & Farhadieh (1971) and Farhadieh & Tankin (1972, 1974). The only modification to the test section was that carborundum particles were deposited on the interior surfaces of the top and bottom plates. This deposit reduces the supercooling required for freezing by providing nucleation sites, but, more important, it greatly improves the reproducibility of the cold-plate temperature (to within $\pm 0{\cdot}2$ °C for a given salinity) at the instant freezing begins.

The experiments may be divided into two general categories.

(i) Sea water, freezing from above. In these experiments, water of greater density lies over water of lesser density. If one exceeds the critical Rayleigh number (as in these experiments), convective currents are present in the vicinity of the ice–water interface.

(ii) Sea water, freezing from below. In these experiments, water of greater density lies below water of lesser density; thus no convection occurs in the test section.

By comparing the results for (i) and (ii), one can determine the effect, if any, of convection on freezing.

The following procedure was used in all the experiments. The filled test section was maintained at room temperature for several hours prior to the start of the

experiment. This was to assure a uniform temperature in the test fluid. The interferometer was adjusted for infinite fringe spacing. When a temperature or salinity variation occurred in the test section, interference fringes appeared, corresponding to iso-phase-shift contours within the test section. Knowing the phase shift as a function of temperature (or salinity), it is possible to obtain temperature profiles (or salinity profiles) through the test section. The relation between the index of refraction and temperature for sea water was obtained by calibration of the system. The relation between the index of refraction and salinity is given by Montgomery (1955).

Cooling water from a constant-temperature bath was circulated through the exterior plates attached to the thermoelectric modules, which, in turn, cooled the fluid in the test section (no electrical power was supplied to the thermoelectric devices at this time). Thus the fluid in the test section was brought to a pre-selected uniform temperature (determined by the bath temperature). It took approximately 2 h to obtain a uniform temperature within the test section. This was assured by the return of the infinite fringe pattern on the interferogram.

In the case of freezing from above, the top plate was cooled and the bottom plate heated (equally) by the thermoelectric modules until the top plate reached the equilibrium freezing temperature or the temperature at which the density of the sea water was a maximum. Although the fluid in the test section was potentially unstable, for these experiments the critical Rayleigh number was not reached (owing to the initial temperature of the test section as determined by the bath temperature). To develop two-dimensional rolls, the top-plate temperature was maintained constant and the bottom-plate temperature increased. The heat flux to the bottom plate was increased in small increments, so that the change in the bottom-plate temperature was less than 0·3 °C/h. Quasi-steady convective rolls formed in the test section when the critical Rayleigh number was exceeded. Once these rolls were well established, further increases in the heat flux to the bottom plate were no longer critical. Eventually a strong convective pattern appeared. This was evidenced by a reversal in the isotherm pattern as seen in figure 1 (*a*) (plate 1). To bring about freezing, the top plate must be supercooled, which may cause a stable layer to develop in the vicinity of the top plate. The depth of this stable layer depends on the salinity of the test fluid, the supercooling required and the cooling rate at the top plate. A stable layer in the test section reduces the intensity of the convective currents by reducing the Rayleigh number. To induce freezing, without allowing a stable layer to grow significantly, the electrical power to the thermoelectric devices attached to the top plate was suddenly increased (to either 5, 7 or 10 A). This electrical current was maintained until the end of the experiment. Just before freezing began, as determined by the top-plate temperature, a movie camera was started.

In the case of freezing from below, the procedure was essentially the same as for freezing from above except that the plate temperatures were reversed and convective currents were not present in the test section. In these experiments, the initial rate of heat addition was not critical. All that was necessary was to be certain that each interval between incremental increases in heat flux exceeded the thermal diffusion time.

Sea water of three salinities was used in these experiments: 18‰, 25‰ and 35‰. This water was obtained from the Shedd Aquarium in Chicago (originally from the Gulf of Mexico) and its salinity was adjusted to the above values by adding either sodium chloride or distilled water. These salinities were chosen for the following reasons. In the case of 18‰ salinity, the equilibrium freezing temperature ($-1{\cdot}2\,^{\circ}C$) lies below the temperature at maximum density ($0{\cdot}2\,^{\circ}C$); for 25‰ salinity, the equilibrium freezing temperature equals the temperature at maximum density ($-1{\cdot}5\,^{\circ}C$); and, for 35‰ salinity, the equilibrium freezing temperature ($-2\,^{\circ}C$) lies above the temperature at maximum density ($-3{\cdot}8\,^{\circ}C$). When freezing from above, sea water of 18‰ salinity will always have a stable layer at the top plate, sea water of 25‰ salinity will have a stable layer if supercooling is required, and sea water of 35 ‰ salinity will have a stable layer if supercooling exceeds $1{\cdot}8\,^{\circ}C$.

3. Results

Figure 1 (plates 1 and 2) is a sequence of interferograms and shadowgraphs showing freezing of sea water (25‰ salinity) from above. Similar results were obtained for salinities of 18 ‰ and 35 ‰. Figure 1 (*a*) shows the isotherm pattern just before freezing; temperature reversal is clearly visible on this interferogram. In figures 1 (*b*) and (*c*), freezing has begun and the ice front is moving downwards from the top plate. A shadowgraph taken 1 s later (figure 1*d*) shows more clearly the shape of the ice–water interface. The peaks and troughs in the interface are aligned with the isotherm pattern. In the troughs of the isotherm pattern, cold water is moving downwards; in the peaks, warm water is moving upwards. Figure 1 (*k*) shows the isotherm pattern much later (about 40 s after freezing began); from this interferogram it can be seen that the convective currents have been greatly reduced. This is primarily due to a reduction in the depth of the test section, which reduces the Rayleigh number significantly. Figure 1 (*k*) also shows the emergence of a salt plume (distortion within fringe pattern) from the ice–water interface (the dependence of the index of refraction on salinity will be discussed later). The first salt plume always originates from a peak in the ice–water interface. Later, the salt plumes appear to originate from random sites on the interface. When freezing of sea water occurs from below, the isotherms are straight and horizontal (no convection is present), and the ice–water interface is flat, without ridges. A total of 35 experimental tests were conducted from which data were analysed.

4. Discussion of results

The shape of the ice–water interface is coupled to the isotherm pattern that exists in the water in the vicinity of the interface. The following data were obtained from the interferograms and shadowgraphs: temperature profiles in the water just before freezing, the temperature at the ice–water interface as a function of time, the penetration of the ice–water interface as a function of time, and the salinity profile within the salt plume.

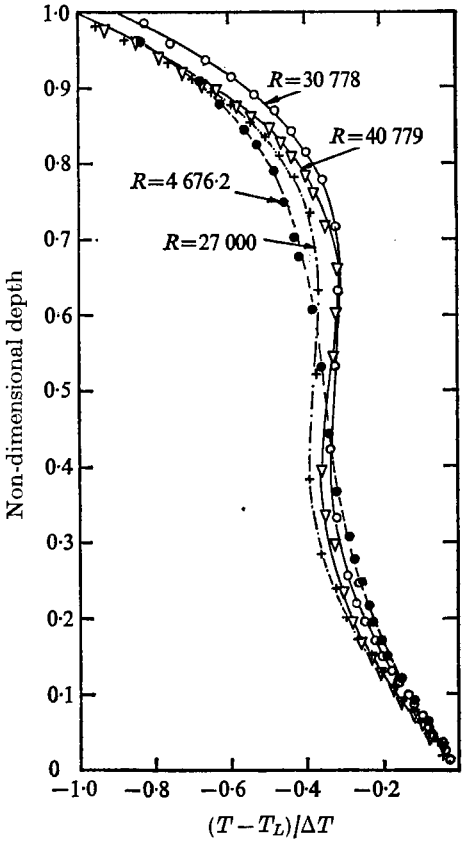

FIGURE 2. Typical non-dimensional temperature profiles obtained just before freezing. Freezing power into top plate = 7 A, Pr = 13. Salinity (‰): ●, 0; +, 18; ○, 25; ▽, 35.

The non-dimensional temperature profiles shown in figure 2 were obtained from the interferograms just before freezing began at the top plate. These four curves represent the temperature profiles for different salinities with the same power input (7 A) to the top plate. Similar results were obtained for 5 and 10 A inputs. These horizontally averaged temperature profiles are explained by Veronis (1966) in his theoretical analysis and by Farhadieh & Tankin (1974). As may be seen, these temperature profiles are not symmetric about the midpoint (−0·5, 0·5). This asymmetry is attributed to two factors. First, a stable layer existed near the top plate (above the unstable layer); thus the layer of conductive heat transfer at the top plate was larger than that at the bottom plate. This tends to shift the temperature profile in the convective region to the right and downwards. Second, the freezing experiment was a transient one. A much greater heat flux was imposed at the top (cold) plate than at the bottom plate. A large power input was supplied to the thermoelectric modules attached to the top plate (7 A) to induce freezing, whereas the bottom plate was merely maintained at constant temperature. Therefore, the temperature gradient in the conductive layer at the top plate was greater than that at the bottom plate, which shifts the temperature

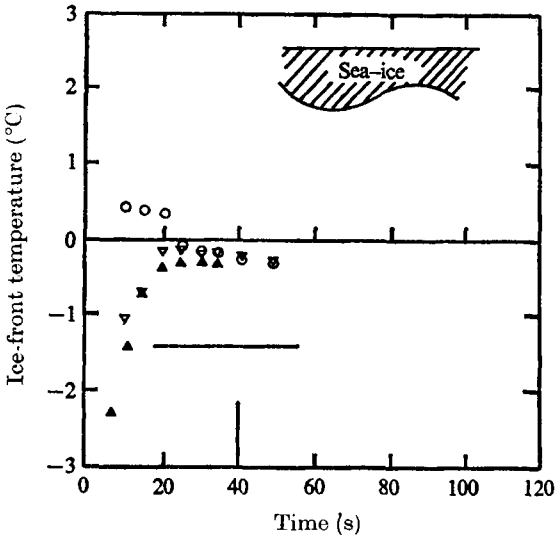

FIGURE 3. Temperature of ice–water interface as a function of time. Horizontal line, equilibrium freezing temperature; vertical line, instant of salt ejection; ○, peak; ▽, trough; ▲, freezing from bottom.

profile in the convective region to the right. The net result of these two effects is a noticeable shift of the temperature profile in the convective region to the right (i.e. the temperature profile does not pass through the midpoint $(-0{\cdot}5, 0{\cdot}5)$).

The temperature overshoot and the thickness of the convective layer seen in figure 2 are indications of the intensity of the convective currents. A better measure of the strength of convection is given by a modified Rayleigh number defined by Sun, Tien & Yen (1969):

$$R = 2g\alpha_1(\Delta T)^2 d^3 A/\nu k,$$

where α_1 is the coefficient of volume expansion $[\rho = \rho_0(1+\alpha_1(\Delta T)^2)]$ and $A = (T_L - T_m)/(T_u - T_L)$ (T_u = top-plate temperature, T_L = bottom-plate temperature and T_m = temperature at maximum density). A value of this modified Rayleigh number is assigned to each of the curves shown in figure 2. The significance of this Rayleigh number (measured just before freezing) with regard to freezing will be discussed later.

Figure 3 is a typical plot of the temperature at the ice–water interface as a function of time for sea water having a salinity of 25‰. This temperature was obtained by counting fringes from the bottom plate, which was used to give a reference temperature (measured with thermistors and recorded on a strip-chart recorder). Temperatures from the interferograms were measured at two points on the interface: a peak and a trough. Initially the temperature at the trough was lower than the peak temperature. A possible explanation is that the convective currents in the sea water at the trough (in the interface) were upward and those at the peak downward. Thus the advance of the ice–water interface at the trough is retarded by convective currents, whereas the advance at the peak is aided by convective currents. On this basis, the trough temperature would be expected

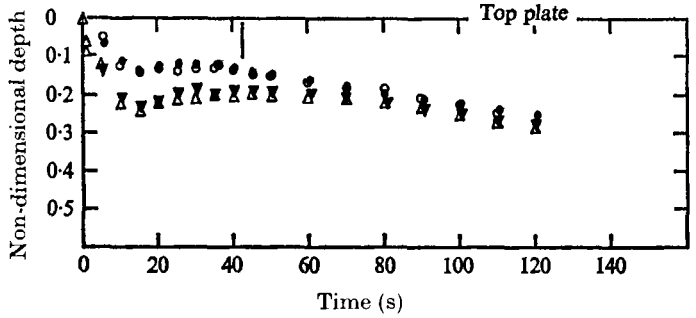

FIGURE 4. Depth of penetration of the ice–water interface as a function of time. Measurements made at the peak (triangles) and trough (circles) of the interface. Vertical line, first instant of salt ejection; solid symbols, shadowgraph; open symbols, interferogram. Salinity = 25 ‰.

to be lower than the peak temperature. About 30 s after freezing began, the interface closely followed the isotherm pattern. This may be seen in figure 3, where the trough and peak temperatures are the same and would correspond to an interferogram taken between those shown in figures 1 (*e*) and (*g*). In all the experiments, the ice–water interface temperature rose with the initial penetration of the front, reached a temperature (about 0 °C) well above the equilibrium freezing temperature ($-1{\cdot}05$ °C for 18‰, $-1{\cdot}5$ °C for 25‰ and $-2{\cdot}5$ °C for 30‰) then slowly dropped (see figure 3). Temperature measurements at the interface had to be terminated when the fringe pattern became badly distorted by the ejection of high salinity brine from the ice. To eliminate the effect of convection, sea water was also frozen from below. The temperature at the interface for these measurements agrees with those obtained by freezing from above (see solid data points in figure 3). Measurements on freezing from below could not be continued beyond about 50 s because the fringe pattern in the vicinity of the ice–water interface became distorted. It is believed this distortion was due to brine ejection, which distributed itself at the ice front, thus indicating that brine ejection is not solely a gravity phenomenon. Similar results were obtained when the experiments were repeated for sea water of salinities 18 and 35‰. The maximum error in temperature measurements at the ice–water interface is $\pm 0{\cdot}4$ °C: the accuracy of the thermistor measurements (plate temperatures) is $\pm 0{\cdot}2$ °C and the error due to fringe counting is at most $\pm 0{\cdot}2$ °C. These two errors are independent of each other, and after examining the scatter in the data from the various experiments, it was concluded that the ice front initially extends to $0\,°C \pm 0{\cdot}2$ °C.

The depth of penetration of the ice–water interface was obtained by examination of the films with an optical comparator. Measurements were made of both shadowgraphs and interferograms and plotted as a function of time. Figure 4 is a typical set of curves showing the results of an experiment with sea water having a salinity of 25‰. Again the measurement points on the interface were in the peak and trough regions. It may be seen that a local maximum penetration of the interface occurred at about 15 s after freezing began. Then the interface at both peak and trough region retreated, the peak retreating faster than the trough. During

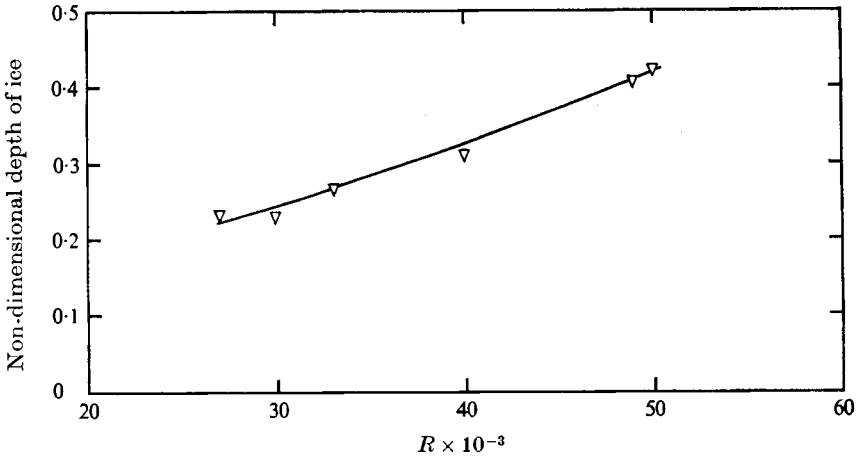

FIGURE 5. Plot of maximum depth of initial advance of ice front as a function of Rayleigh number prior to freezing.

this initial period of penetration and retreat, the interface was dendritic in structure (figures 1 *b–f*). However, with melting at the interface and perhaps consolidation within the ice layer, the interface became relatively smooth (see figures 1 *g, h*). About 40 s after freezing, the interface began to readvance, and, about 60 s after freezing began, the interface became essentially flat. The results shown in figure 4 are characteristic of all the experiments. The maximum depth of initial penetration of the interface correlates rather well with the Rayleigh number just before freezing began. This correlation is shown in figure 5. These data points include results for sea water of various salinities, test sections of various depths and freezing at various heat fluxes. In summary, the convective currents in water just before freezing appear to be significant in determining the maximum depth of the initial penetration of the ice–water interface.

The salt plume that first appeared in the freezing sea water originated from a peak in the ice–water interface. The time from the instant that freezing began until the first salt plume was observed varied from one experiment to another. One cannot assume that the first salt plume observed was the first to appear in the test section, since less than one-quarter of the test section was visible, nor that salt plumes did not appear simultaneously from several of the peaks in the interface. All that can be reported is that, in every experiment conducted, the first salt plume observed originated from a peak in the ice–water interface shortly after the interface began its retreat (see 'start of salt ejection' in figure 4). Later, salt plumes appeared at random points on the interface and greatly distorted the fringe pattern. The salt plumes appeared to originate from channels in the ice, and not from a layer of high salinity brine at the interface as reported by Foster (1969). No such layer of brine was ever detected. If such a layer was present, it should appear clearly on the interferogram. Our finding that the salt plume first appeared at a preferential site (a peak in the interface) is contrary to what we reported in an earlier paper (Farhadieh & Tankin 1972). We believe that this is due to the fact that two-dimensional rolls were not established in the test section

in the earlier experiment. It may be expected that the convection in the sea water has an effect on the alignment of the ice crystals at the interface during freezing. High salinity brine, which is ejected from the ice, is located in channels between the ice crystals. Thus, if the ice crystals at the peak region of the ice–water interface were pointing downwards (convection is downwards at such sites), then one would expect brine to be ejected (salt plume) first from a peak in the interface, which is what happens. However this is conjecture; the experimental set-up does not allow microscopic examination of the ice.

Figure 6 (plate 3) is an enlargement of an interferogram (such as figure 1 *k*) showing the localized distortion in the fringes caused by a salt plume. The horizontal line inscribed on the interferogram is the vertical location in the test section where the analysis is to be made. It may be seen that a fringe shift of approximately one fringe occurs owing to the salt plume. This fringe shift is caused primarily by the salinity variation in the salt plume and not temperature variation. The reason for this is as follows. For an optical path of about 0·15 cm (measured diameter of salt plume), a temperature variation (in the vicinity of 0 °C) greater than 10 °C is required to produce a single fringe shift, whereas a salinity change of 0·1 ‰ over a distance of 0·15 cm can produce a single fringe shift. The brine in a salt plume comes from an ice front which is at a temperature of about 0 °C; thus the temperature variation between the salt plume and the ambient sea water (where the analysis is made) is at most $1\frac{1}{2}$ °C. Thus temperature effects would cause a fringe shift of less than 0·15 fringes. Therefore it is assumed that in the salt plume the temperature effects on the fringe shift can be neglected compared with the salinity effects.

The method of analysis involves the use of Abel inversion techniques. Axial symmetry is assumed, that is each horizontal cross-section of the salt finger is assumed to be a circle. In a cross-section, x represents the lateral distance from the axis of symmetry and y is the co-ordinate along the line of sight (normal to x). Let us denote the lateral fringe shift by $S(x)$. The object is to find a relation between $S(x)$ and $S(r)$, the radial fringe shift within the salt plume. Assuming that the fringe shifts in the salt plume are additive, which is justified, the lateral fringe shift is given in terms of the radial fringe shift by the integral

$$S(x) = 2\int_0^Y S(r)\,dy,$$

where Y is the value of y on the boundary of the circular cross-section, of radius R. By transforming co-ordinates, the following relation is obtained:

$$S(x) = 2\int_0^{(R^2-x^2)^{\frac{1}{2}}} \frac{rS(r)\,dr}{(r^2-x^2)^{\frac{1}{2}}}.$$

This is the Abel integral equation, which can be solved analytically, giving

$$S(r) = -\frac{1}{\pi}\int_r^R \frac{S'(x)\,dx}{(r^2-x^2)^{\frac{1}{2}}},$$

where $S'(x)$ is the derivative of $S(x)$ with respect to x. Standard numerical techniques are available to evaluate the Abel integral equation.

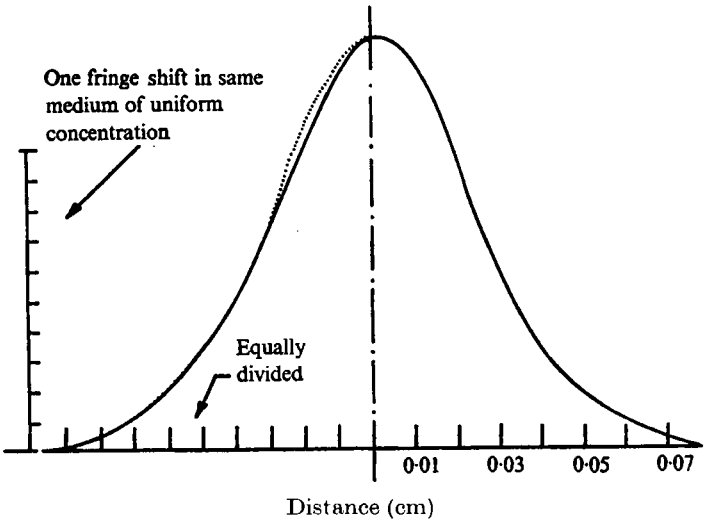

FIGURE 7. Lateral distortion $S(x)$ in fringe caused by salt plume. ——, lateral fringe shift; ·····, folded curve. Salinity of sea water = 25 ‰.

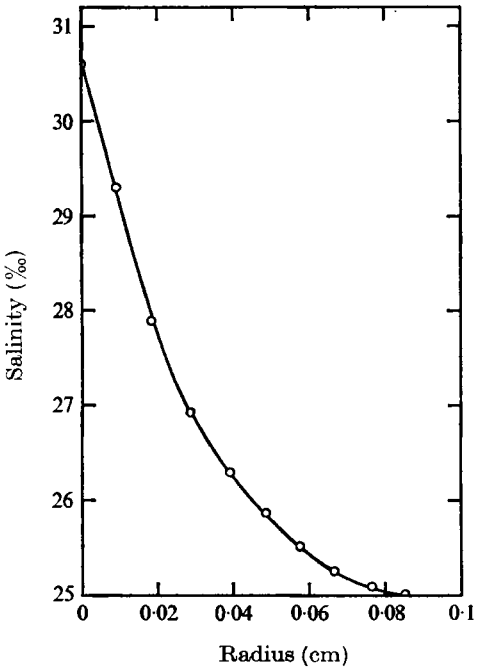

FIGURE 8. Radial distribution of salinity within salt plume. Sea water: salinity = 25 ‰, depth = 0·9525 cm. Freezing power into top plate = 7 A.

Figure 7 shows the lateral distribution $S(x)$ of the fringe shift. These data were taken from the interferogram in figure 6, where measurements of $S(x)$ were taken at 0·0025 in. intervals across the salt plume. This curve was folded about its centre-line, and the dotted curve shown in figure 7 is the horizontally averaged profile that is used in Abel inversion. From the computed radial fringe shift $S(r)$,

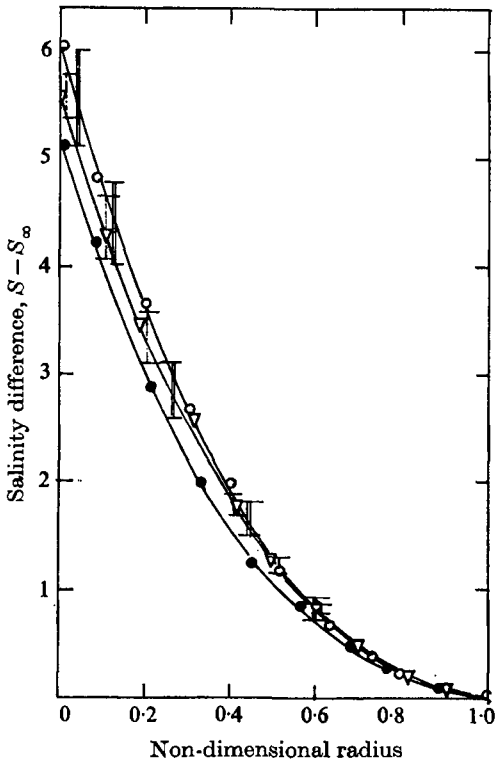

FIGURE 9. Radial distributions of salinity in salt plumes above ambient sea-water salinity S_∞. ○, $S_\infty = 35$ ‰; ▽, $S_\infty = 25$ ‰; ●, $S_\infty = 18$ ‰. Freezing power into top plate = 7 A.

the salinity as a function of radius is obtained. This result is shown in figure 8. The salinity increases across the salt plume, reaching a maximum at the centre-line. The centre-line salinity of the salt plume is about 5½‰ above the ambient salinity.

Radial salinity profiles in salt plumes were obtained for various salinities. The results of these experiments are shown in figure 9. It may be seen that the increases in salinity above the ambient value are approximately the same. The error bars associated with sea water of salinity 25‰ were obtained by folding the lateral data about different centre-line values and then inverting them. The possible errors in the data exceed the variation between the three experiments. From these results one can estimate the salinity within the brine channels in the ice during early stages of freezing to be about 5½‰ above the ambient salinity of the sea water.

It appears that the only method for obtaining salinity profiles within the salt plume is by optical techniques such as those used in this study. Since the salt plumes are only about a millimetre in diameter it would be difficult to make a probe small enough to traverse the plume without causing significant disturbance.

5. Conclusions

(i) In the early stages of freezing, when convection currents are relatively strong, the interface does not follow exactly the isotherm pattern in the fluid. This is due to the convection currents present in the fluid. At later stages of freezing the isotherm pattern and interface agree.

(ii) During early stages of freezing, the temperature at the ice–water interface is not the equilibrium freezing temperature. For sea water of salinities 18, 25 and 35‰, the interface temperature was approximately 0 °C, whereas the equilibrium freezing temperatures for these fluids are −1·05 °C, −1·5 °C and −2·05 °C respectively.

(iii) The maximum depth of the initial penetration of the ice–water interface (before retreating) depends on the degree of supercooling and strength of the convection currents in the sea water (Rayleigh number) just before freezing.

(iv) The first salt plume observed always appears at a peak in the ice–water interface.

(v) The salinity profile in the salt plume was measured and its centre-line value was approximately 5½‰ above the ambient salinity of the sea water. This centre-line salinity is an indication of the salinity in the brine channels within the ice.

The Office of Naval Research provided financial support for this study under Contract N00014-67-A-0356-0021. The authors appreciate the many helpful suggestions of A. Hanson and J. Witting.

REFERENCES

BOGER, D. V. & WESTWATER, J. W. 1967 *Trans. A.S.M.E., J. Heat Transfer*, C **89**, 81–89.

FARHADIEH, R. & TANKIN, R. S. 1972 *J. Geophys. Res.* **77**, 1647–1657.

FARHADIEH, R. & TANKIN, R. S. 1974 *J. Fluid Mech.* **66**, 739–752.

FOSTER, T. D. 1969 *J. Geophys. Res.* **74**, 6967–6974.

HEITZ, W. L. & WESTWATER, J. W. 1971 *Trans. A.S.M.E., J. Heat Transfer*, C **93**, 188–196.

MONTGOMERY, R. B. 1955 *American Institute of Physics Handbook*, 2nd edn, pp. 2–123.

ROYAL, J. W. 1969 Ph.D. dissertation, Boston University.

SUN, Z. S., TIEN, C. & YEN, Y. C. 1969 *A.I.Ch.E. J.* **15**, 910.

TANKIN, R. S. & FARHADIEH, R. 1971 *Int. J. Heat Mass Transfer*, **14**, 953–961.

TIEN, C. & YEN, Y. C. 1966 *Chem. Engng Prog. Symp.* **62**, 166–172.

TOWNSEND, A. A. 1964 *Quart. J. Roy. Met. Soc.* **90**, 248–259.

VERONIS, G. 1966 *J. Fluid Mech.* **26**, 49–68.

YEN, Y. C. 1968 *Phys. Fluids*, **11**, 1263–1270.

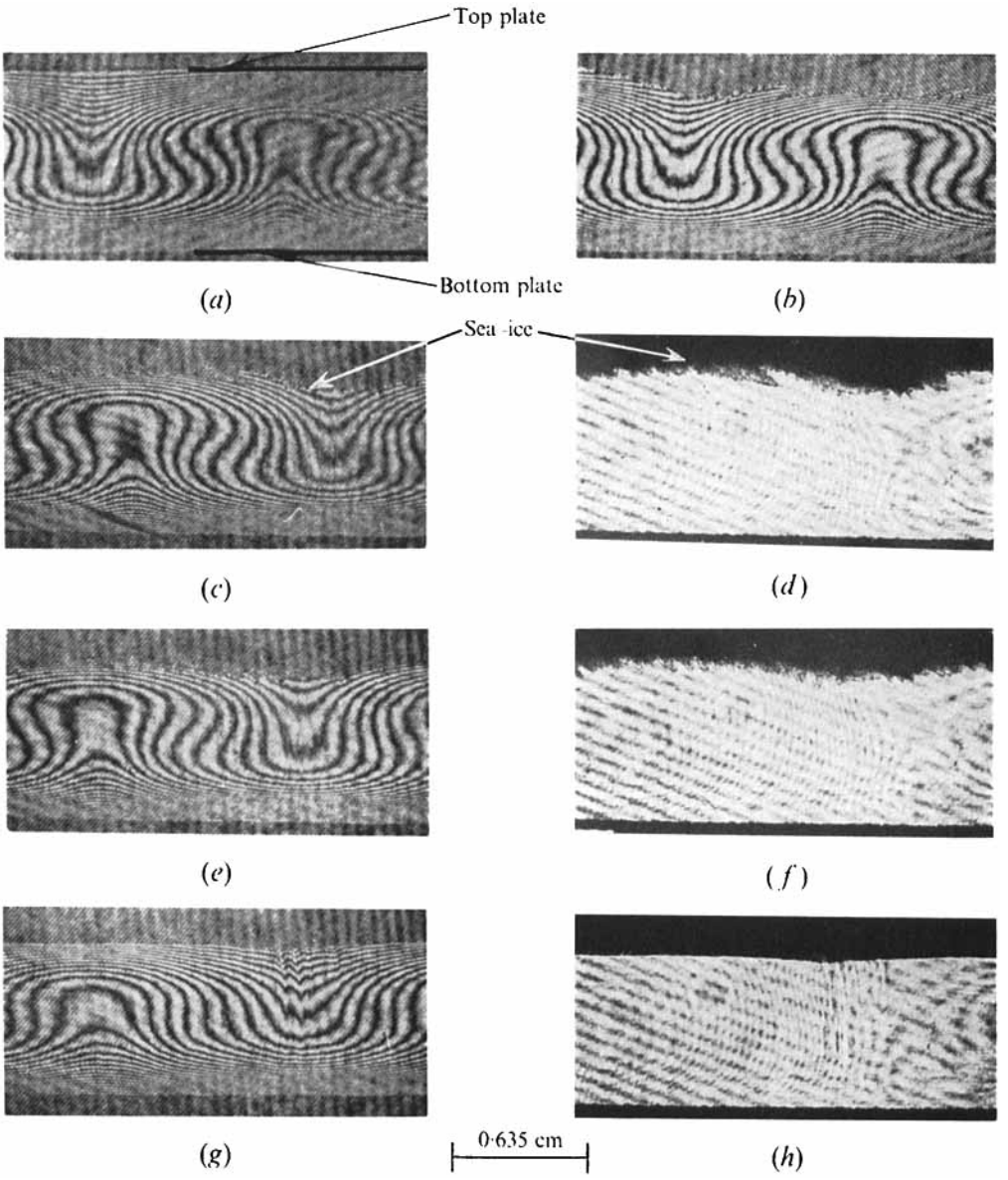

FIGURES 1 (*a–h*). For legend see plate 2.

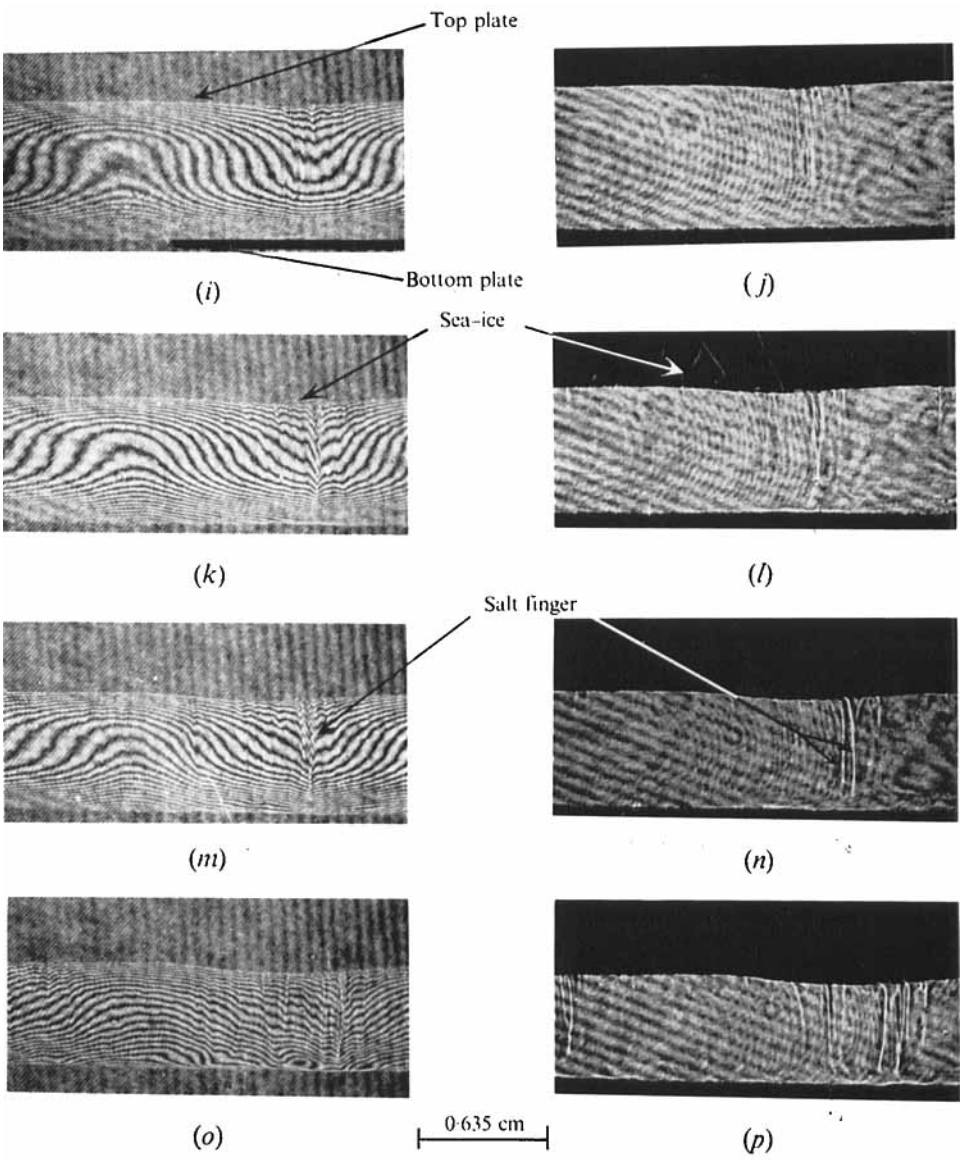

FIGURE 1. Sequence of interferograms (*a, c, e, g, i, k, m, o*) and shadowgraphs (*d, f, h, j, l, n, p*) showing freezing from top plate. Salinity = 25‰.

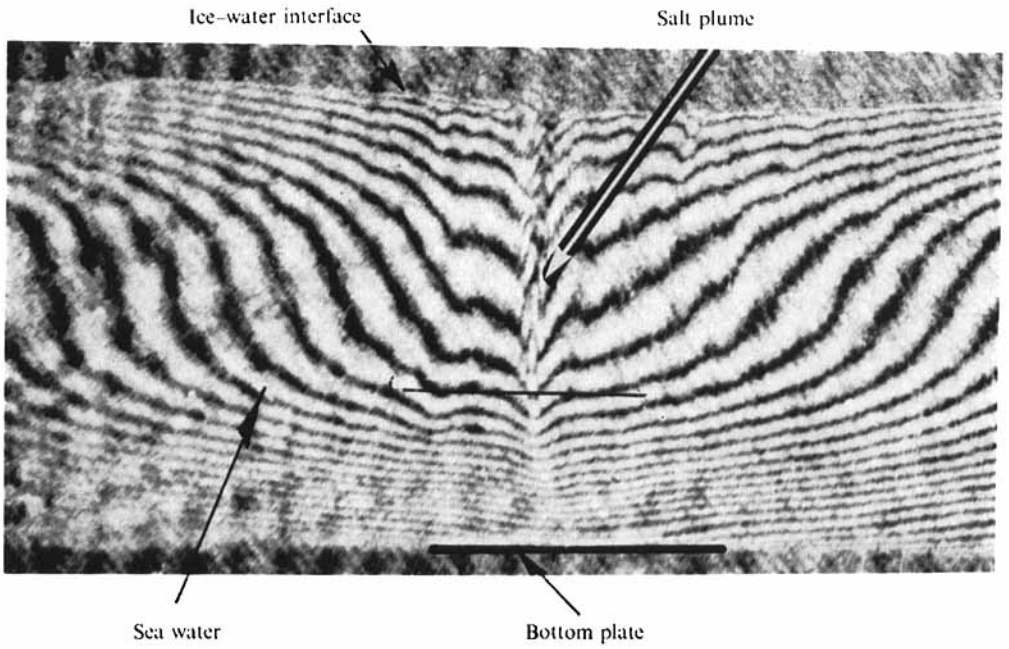

FIGURE 6. Interferogram showing salt plume. The unmarked horizontal line indicates the elevation where the lateral data were taken.